Driving Forces of Cationic Dye Adsorption, Confinement, and Long-Range Correlation in Zeolitic Materials

Marwa Assaf, Gaelle Martin-Gassin, Benedicte Prelot, Pierre-Marie Gassin

The Driving Forces of Cationic Dye Adsorption, Confinement and Long Range Correlation in Zeolitic Materials

Marwa Assaf [a], *Gaelle Martin-Gassin*[a], *Benedicte Prelot*[a], *Pierre-Marie Gassin*[a]*

[a] ICGM, Univ Montpellier, ENSCM, CNRS, 34095 Montpellier, France

Corresponding Author:

*pierre-marie.gassin@enscm.fr

KEYWORDS Faujasite – Adsorption - Second Harmonic Scattering - Solvent effect – hemicyanine dye - Cationic Exchange Capacity – Solid / Liquid Interface- Isothermal Titration Calorimetry

ABSTRACT

Zeolitic materials are commonly used to capture emergent contaminants in water or in complex aqueous effluents. The efficiency of this adsorption depends strongly on the guest-host interactions and on the surrounding environment with possible co-adsorption of the solvent. Only few experimental techniques are available to probe in situ the sequestration processes at the solid / liquid interface. We propose in the present work to combine Second Harmonic Scattering (SHS)

technique with Isothermal Titration Calorimetry (ITC) in order to investigate the adsorption and the confinement of an hemicyanine dye adsorbed inside Faujasite materials. The methodology described here permits to quantify the correlations between the confined dyes in the material, and thus give local information about the organization at the nanometer scale. Various impacts, such as the effect of solvent type, the silicon to aluminum ratio of the zeolitic adsorbent, are quantitatively estimated and discussed. This work highlights that the most correlated system matches with the higher adsorption capacity associated with the lower entropic contribution.

Introduction

Zeolites, porous crystalline structures of Aluminum Silicate, have great potential for a wide range in technical[1], industrial[2-3], agricultural[4], environmental[5] and biomedical applications[6]. These applications are based on their outstanding properties for sorption, ion-exchange and catalytic processes. Numerous studies have also emphasized the ability of zeolitic material for the purification and the capture of emergent contaminants from water[7-15] or complex beverage like wine[16]. Indeed, in addition to their valuable sorption selectivity, or exchange capacity, these materials otherwise exhibit high chemical stability, good recyclability and above all non-toxicity. Zeolitic materials have been the object of numerous studies to tune their chemistry, their structure, their textural properties, to optimize their efficiency on the one hand [17-19] and to understand the driving force of adsorption and confinement processes on the other hand.

The porous network and the presence of confined spaces bring new properties such as chemical reactivity under nanoconfinement [20] in general and for the case of zeolite their use in heterogeneous catalysis. Indeed, catalytic reactions in confined spaces exhibit unique behaviors compared to those observed on bulk materials [21-22]. The confinement effects thus imply modification on

catalytic reaction, as well as on diffusion and on adsorption/desorption. For application on sorption, there are various properties responsible for the modification of sorption behavior, with the structural and the textural properties together with the surface chemistry. This is particularly the case at the solid / liquid interface with additional physicochemical properties, and where the sorption is indeed a displacement. This involves the influence of the nature of the solvent[23-24] and the specific influence of the hydration of adsorbed and desorbed species [25]. For zeolites, the adsorption properties are governed by the ability of adsorbed molecules to penetrate into zeolite voids and by their surface chemistry, with hydrophilic/hydrophobic balances, surfaces acidities (Lewis and Bronsted), and mainly their permanent charge. This charge is designed as the Cation Exchange Capacity (CEC), resulting from the isomorphic substitution of Silicon atoms by Aluminum within the crystallographic framework. Even if interesting theoretical results are reported concerning the understanding of the Bronsted Acid Site (BAS) role[24, 26-27] in sorption and catalytic properties[28], the various contributions of the mechanisms [28-30] are not commonly investigated from the experimental and local point of view.

The aim of this work is to investigate the guest-host interactions and to rationalize the significance of electrostatic, Van Der Waals and steric interactions in the global adsorption process. To achieve that, the adsorption of a pyridinium iodide salt inside Faujasite materials has been chosen as reference system. The adsorption is studied by modulating the nature of the solvent and the charge inside the material as depicted in Figure 1. To characterize and quantify these interactions, UV-visible absorption method is used to determine the macroscopic adsorption isotherm, Isothermal Titration Calorimetry (ITC) measurement are performed in order to get macroscopic information about the thermodynamic of the adsorption and an original approach based on Second Harmonic Scattering (SHS), is employed to probe the local organization of the

dye inside the material, within the micropores. This last technique, based on Second Harmonic Generation (SHG) phenomena, in which two photons at frequency ω are converted into a photon at the double frequency 2ω, has become increasingly popular since recent studies[31-40] demonstrated that it is suitable to obtained information about organization in long range structured system. Recent works[33, 41-42] have developed a methodology to quantify the correlation between the nonlinear emitter, by analyzing the polarization resolved SHS signal. The novelty of this work is to combine these two approaches, global calorimetric measurement and local SHS measurement used until now to quantify correlation in homogeneous liquid, to probe the order of the guest molecules confinement inside the microporous host material. The hemicyanine dye is chosen because it is an efficient SHG active molecule, and previous works have demonstrated its insertion in zeolitic system[39]. The material studied here is a Faujasite type zeolite which consists of cubic-octahedrons called sodalite cages or β-cages. The assembly of these cages linked together by hexagonal prisms leads into a larger cavity of diameter 13 Å called supercage (SC) which is approximately the size of the guest hemicyanine dye molecule chosen. The β-cages are only accessible to solvent, whereas the supercages are accessible for solvent and organic dye[30].

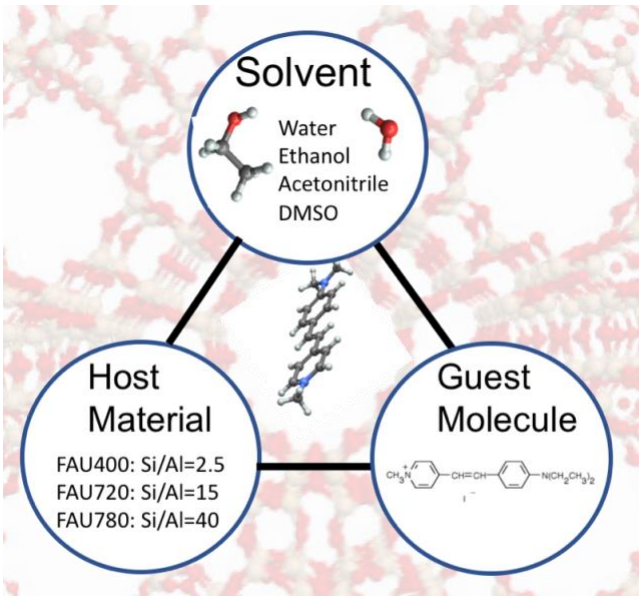

Figure 1. Schematic representation of the three various elements (adsorbate, adsorbent and solvent) involved in the modulation of the adsorption processes and studied in the present work. The hemicyanine dye is referred as sDiA dye molecule in the following.

Experimental procedure

1°) Reagent and materials:

Faujasite Y with different Si/Al ratio were purchased from Zeolyst International: Faujasite CBV400, CBV720, and CBV780 with Si/Al ratio equal to respectively to 2.5, 15 and 40 and referred as FAU400, FAU720 and FAU780 in the following. The materials have been used as received, without modification, and are in the acidic form. The CEC of these different materials are theoretically deduced by the Si/Al ratio and equal to 4.7 $meq.g^{-1}$, 1.0 $meq.g^{-1}$ and 0.4 $meq.g^{-1}$ respectively (additional details are given in the SI, including the XRD patterns).

Acetonitrile, Ethanol, and DMSO were obtained from Sigma Aldrich at HPLC grade. Ultrapure water is 18 MOhm.cm resistivity. The hemicyanine dye is 4-(4-Diethylaminostyryl)-1-methylpyridinium iodide, M=394.29 $g.mol^{-1}$ also refereed as sDia in the following, purchased from Sigma Aldrich. All chemicals were used as received without further purification.

Fresh suspensions of Faujasite in the considered solvent were prepared at a solid / liquid concentration of 0.1 $g.L^{-1}$ and used within 12h. Suspensions were sonicated 10 minutes and kept under constant stirring at 25 °C to prevent solid particles aggregation before using. The characteristic size of all the particles in all solvent is around 800 nm diameter +/- 200 nm determined with DLS (additional details in SI).

2°) Adsorption isotherm:

The adsorption isotherms were determined using the depletion method in batch conditions by putting in contact the Faujasite suspension at 0.05 $g.L^{-1}$ coming from the fresh suspensions and solutions of hemicyanine at various initial concentrations prepared from a 2 mM stock solution. After overnight stirring at 25 °C, the suspensions are centrifugated at 11000 rpm during 1h and then filtered with polypropylene 0.2µm filter. The dye adsorbed onto the material is determined according to:

$$\Gamma_{ads} = \frac{(C_0 - C_e)V}{m} \quad (1)$$

Where Γ_{ads} is the dye amount adsorbed into the material, V is the volume (L) of the solution, and m is the mass of the solid phase (g), C_0 is the initial concentration of the dye and C_e is the equilibrium concentration in the supernatant. This C_e was measured by UV-vis absorbance (JASCO V-670) at 460 nm on the supernatant.

3°) ITC measurements

Isothermal Titration Calorimetry (ITC) measurements were performed with a TAM III multichannel calorimetric device with nanocalorimeters and a Micro Reaction System (TA Waters). Experimental conditions (concentrations, solid /liquid ratio) have been optimized to be in correlation with the adsorption isotherm, and taking into account the technical constraints (cell or syringe volume, solubility of the dye) to ensure that the signal is high enough to be properly detected and quantified, and to reach the complete loading at the end of the experiment. ITC experiments were carried out in cells (hastelloy) with 800 µL of zeolithic suspension, at 298 K and consist of 25 injections of 10 seconds with 10 µL of the dye solution at 2 mM. The system is

equipped with a gold paddle stirrer used at 90 rpm. In order to allow the system to stabilize between injections, the latter are spaced 45 min apart. The dilution effect is evaluated under similar conditions with only the solvent. The global heat effect were calculated after appropriate subtraction of the dilution effect, and then for each injection is has been related to the real adsorbed amount from the isotherm. [43] The final results are represented as the cumulative displacement enthalpy since the enthalpy represents a global effect combining various contributions involved in the overall sorption process including adsorption / exchange, hydration and displacement. [25]

4°) SHS measurement:

The polarization resolved SHS experimental setup is detailed elsewhere[44] and additional details are given in SI. Briefly, the SHS intensity is monitored in the right angle direction as a function of the input polarization angle γ, which was selected with a rotating half-wave plate and the second harmonic light was selected in the vertical state by an analyzer, placed in front of the spectrometer. All experimental data were recorded for 10 s under stirring conditions, a magnetic stirrer is operated in the cell measurement. For each system, two separate SHS measurements are performed. On the one hand, the SHS measurement of the whole suspension and on the other hand, the SHS measurement of the supernatant solution obtained after centrifugation. Formally, the SHS intensity of the suspension comes from 3 different contributions as depicted in formula (2):

$$I^{2\omega}_{suspension}(\gamma) = I^{2\omega}_{HRS,dye}(\gamma) + I^{2\omega}_{HRS,solvent}(\gamma) + I^{2\omega}_{SHS,dye+materials}(\gamma) \quad (2)$$

Where $I^{2\omega}_{HRS,dye}$ is the uncoherent Second Harmonic light coming from the free dye in solution also referred in the literature as the Hyper Rayleigh Scattering (HRS) contribution of the dye;

$I^{2\omega}_{HRS,solvent}$ is the Hyper Rayleigh Scattering contribution of the solvent, and $I^{2\omega}_{SHS,dye+materials}$ is the Second Harmonic light contribution of the dye adsorbed onto and into the material. The contribution of the bare Faujasite can be neglected as it is shown in the additional data presented in SI. The SHS intensity of the supernatant can be written as:

$$I^{2\omega}_{supernatant}(\gamma) = I^{2\omega}_{HRS,dye}(\gamma) + I^{2\omega}_{HRS,solvent}(\gamma) \quad (3).$$

At the concentrations where the SHS experiment are performed, the re-absorption of the 2ω photon by the solution is negligible[45] as it is discussed in SI. Thus, the SHS signal coming from the dye adsorbed onto and into the material is obtained by the subtraction equation (2) minus equation (3):

$$I^{2\omega}_{SHS}(\gamma) = I^{2\omega}_{suspension}(\gamma) - I^{2\omega}_{supernatant}(\gamma) \quad (4)$$

All the SHS data presented in the manuscript are treated according to equation (4).

Results and discussions

1°) The Si/Al ratio effect on the adsorption

Figure 2A shows the adsorption isotherms of sDiA in water onto the different faujasite materials. According to the nature of the initial portion of the curve and its slope, the isotherms exhibit a shape corresponding to a L type (or Langmuir type) following Giles classification. The adsorption isotherms are thus well fitted with the Langmuir like model, equation (5), even if liquid-phase adsorption of molecule into zeolites is not a situation traditionally characteristic of a Langmuir isotherm. The applicability of this model is discussed here[24] and results from a relatively strong interaction of the dyes with the pore walls.

$$\Gamma_{ads} = \frac{\Gamma_{max} C_e K_L}{1 + C_e K_L} \quad (5)$$

Through this simplified adsorption model used in its linearized form, the maximum amount of adsorbed dye Γ_{max}, as well as the Langmuir constant K_L have been evaluated for sDiA sorption on the various zeolites. For the sDiA adsorption, the maximum amount capacity varies from 0.622 mmol.g^{-1} for the FAU400 material, to 0.338 mmol.g^{-1} for FAU780 material. This finding is explained by the number of adsorption sites available depending on the Si/Al ratio of the material. Indeed, these adsorption sites are located on the oxygen atom neighboring an aluminum atom and are thus refereed as Brønsted Acid Site (BAS)[24, 26-27, 46]. The different material FAU400, FAU720 and FAU780 exhibits different BAS number, or it is the same thing different CEC, which are respectively equal to 4.7 meq.g^{-1} (6.7 sites per SC), 1.0 meq.g^{-1} (1.5 sites per SC) and 0.4 meq.g^{-1} (0.6 sites per SC). For FAU780 material, the BAS amount limits the adsorption process because the Γ_{max} measured to 0.49 molecule per SC is close to the theoretical CEC of 0.59 site per SC. It confirms that the cationic exchange is the driving force of the adsorption, and that other interactions like Van der Waals interaction are not efficient to yield dye adsorption. At higher charge density in the material, the adsorption is limited by the empty space available in the pore. When the ratio of 1 molecule per SC is reached, no more adsorption can occur even if there is more BAS. The adsorption capacity Γ_{max} is nearly the same for FAU720 and FAU400 materials, around 1 molecule adsorbed per SC, far lower from the theoretical CEC of 6.7 sites per SC for FAU400. It shows that the amount adsorbed depends on the number of available exchange sites, with a maximum limit due to the steric hindrance because of the size of the adsorbate.

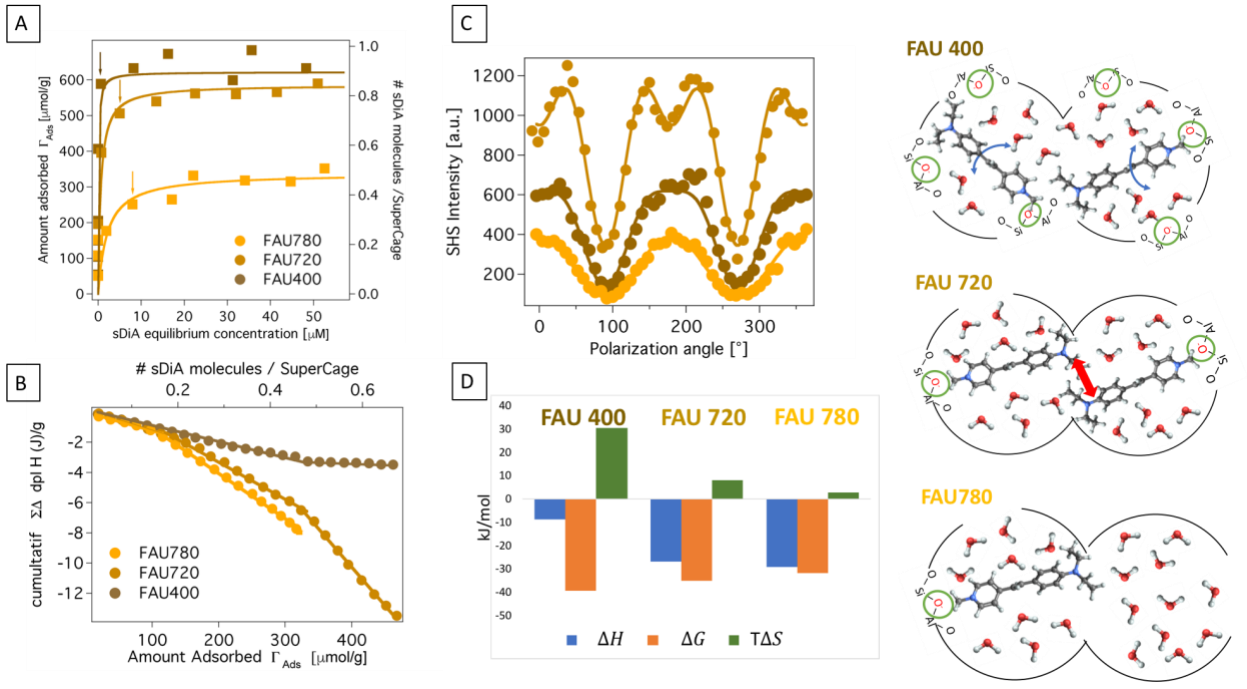

Figure 2. A) sDiA in water adsorption isotherm onto the three Faujasite, B) Corresponding ITC measurement, C) SHS polarization plot measured at the concentration given by the arrow in A), D) the adsorption thermodynamic quantities for the three Faujasite, at high coverage. On right, a microscopic picture to illustrate the interaction or not between the neighboring dyes.

Figure 2B shows the displacement enthalpy measured by ITC during the adsorption process on the three different materials. The observed behavior is different for the various considered materials. ITC approach provides the chance to measure directly the heat effect all along the isotherm. The displacement enthalpy is determined for various surface coverage corresponding to the complete loading of the materials. Three 3 distinct areas can be observed depending on the amount adsorbed range. In the first region, at low adsorption, *i.e.* when Γ_{ads} < 0.2 molecule per SC, the displacement enthalpy, obtained by the slope in the graphic 2B, is the same for the 3

materials with a value around ΔH_{ads} = -10 kJ.mol^{-1}. In the intermediate region, 0.2 < Γ_{ads} < 0.5 molecule per SC, the displacement enthalpy is nearly stable for FAU400, but it increases for FAU720 and 780 at around ΔH_{ads} = -28 kJ.mol^{-1}. In the high adsorption region, this quantity continues to increase for FAU720 with high ΔH estimated at -50 kJ.mol^{-1}, whereas it slightly decreases for FAU400. For FAU780 at sorption higher than 0.32 mmol.g^{-1}, calculation does make sense since saturation is reached and no adsorption occurs. Those results can be discussed with a microscopic model that supposed independent filling of the SC from the neighboring SC. Indeed, in each Faujasite material, a SC is linked by a dodecagonal window to four other SC. In the low adsorption region, the adsorbed dye is in average involved in a SC surrounded by four empty SC. Thus, no interaction between the dye occurs in this regime. At higher adsorption, 0.2 < Γ_{ads} < 0.5 molecule per SC, an adsorbed dye begin to interact with another dye located in a neighboring SC. For FAU720 and FAU780 material, the increase in the displacement enthalpy may be explained by this interaction. On the contrary, for FAU400 material, the presence of unoccupied sites could change this behavior with more spatial configuration available for the adsorption as depicted in Figure 2 right. To go further in the thermodynamics, the enthalpy measurements are compared with other thermodynamics quantities. As the system is a dilute solution of a charged adsorbate, the global free adsorption enthalpy ΔG_{ads} can be deduced from the constant extracted from equation (5) applied to the adsorption isotherm [47]:

$$\Delta G_{ads} = -RTln(K_L) \quad (6).$$

An estimation of the entropic term $T\Delta S_{ads}$ can be done with the combination of the measured ΔH_{ads} from ITC and the calculated ΔG_{ads}. The results are given in table 1 and Figure 2D. Two ranges on the surface coverages have been distinguished, with Γ_{ads} lower or higher than 0.2 molecule per SC.

For low surface coverage, the entropic terms $T\Delta S_{ads}$ is in the range of 30-20 kJ.mol^{-1} for the 3 materials, with a slight decrease from CBV-400 to CBV-780 in line with the small decrease of ΔG_{ads}. For higher loading, the difference in the entropic contribution between materials is more pronounced, with a high decrease of $T\Delta S_{ads}$ for CBV-400 to CBV-780. FAU400 and FAU720 exhibit nearly the same adsorption capacity, but the adsorption thermodynamics quantities are strongly different with a higher entropic contribution for the FAU400. As mentioned above, this difference should be attributed to the presence of unoccupied sites. To probe locally the order/disorder of the dye organization inside the material, polarization resolved SHS measurement are presented in figure 2C. These data were analyzed as a Fourier series[33]:

$$I_{SHS}(\gamma) = i_0 + i_2 \cos(2\gamma) + i_4 \cos(4\gamma) \quad (7)$$

where i_0, i_2 and i_4 are the amplitudes of the constant, the harmonic 2γ and the harmonic 4γ terms. In Eq. (7), the parameters i_0 and i_2 are related to the local microscopic structure, i.e. the first hyperpolarizability of the dye and i_4 to the long-range correlations. In the case of uncorrelated species, SHS is a purely incoherent phenomenon and the amplitude i_4 vanishes[33]. On the contrary, when molecular orientations are correlated, the scattered photons have well-defined phase relationship and i_4 differs from 0. To quantify this term, the normalized parameter I_4 is introduced as :

$$I_4 = \frac{i_4}{i_0} \quad (8)$$

I_4 is equal to 0 when no correlation occurs between adsorbed dyes and is different from 0 when correlations between dyes exist. The I_4 parameter deduced from the fit are presented in Table 1 and its absolute value is clearly higher for FAU720 compared to FAU400 and FAU780. As

discussed above, FAU400 and FAU720 exhibit nearly the same filling of the material, and the higher I_4 value for the FAU720 is puzzling. This trend is in line with the higher FAU400 entropic contribution and the most convincing explanation involves the unoccupied sites. For FAU 400 material, the dye molecule may probably change from one configuration to other one and for FAU720 the dye molecule is most confined as depicted in Figure 2 right. Thus, at high loading, unoccupied sites result in a loss of long range order and in a lower value for I4.

Table 1. Results of the fitting parameters extracted from macroscopic experiment adsorption of sDiA, with the Γ_{max}, the maximum amount adsorbed, K_L the Langmuir like constant, ΔG_{ads} the corresponding free enthalpy obtained from equation (6), ΔH_{ads} measured by ITC, deduced $T\Delta S_{ads}$ and I_4 the normalized SHS correlation parameter. For ΔH_{ads} and $T\Delta S_{ads}$, the values are calculated for the two various regimes, with low surface coverage (in *italic*) and high surface coverage (in **bold**).

Material	Γ_{max} [μmol.g^{-1}]	Γ_{max} [molecule/SC]	K_L [L.μmol^{-1}]	ΔG_{ads} [kJ.mol^{-1}]	ΔH_{ads} [kJ.mol^{-1}]	$T\Delta S_{ads}$ [kJ.mol^{-1}]	SHS-I_4 parameter
FAU400	622	0.9	10	-39.3	*-9.3*	*30.0*	- 0.10
					-8.7	**30.6**	
FAU720	588	0.85	1.7	-34.9	*-11.0*	*23.9*	- 0.26
					-26.7	**8.2**	
FAU780	338	0.49	0.5	-31.9	*-12.1*	*19.8*	- 0.01
					-29.2	**2.7**	

2°) The solvent effect on the adsorption

Figure 3A shows the sDiA adsorption isotherms onto the FAU720 material with different solvents. The maximum amount of adsorption varies with the solvent in the order Water>acetonitrile>Ethanol>DMSO. Those results follow the order recently published[24] obtained with pyridine onto various zeolites. These findings are explained by the efficiency of the exchange which depends on the ionic properties of the solvent. Indeed, if the proton is solvated, as depicted in Figure 3C, the cationic exchange occurs, and not on the otherwise. For the water solvent, Γ_{max} reaches nearly the CEC, which means that BAS can be considered as "active" for the exchange. For the other solvents, Γ_{max} is lower than the CEC, and the BAS are partially "inactive" in respect with the lower relative permittivity value of the solvent. As depicted in figures 3C and 3D, the solvent effect could be explained by this difference in proton solvation. Figures 3 B presents the SHS polarization plots for these systems. The case of water solvent exhibits a significative I_4 contribution, as discussed above. All the other SHS polarization plots show a nearly zero I_4 contribution as summarized in Figure 5.

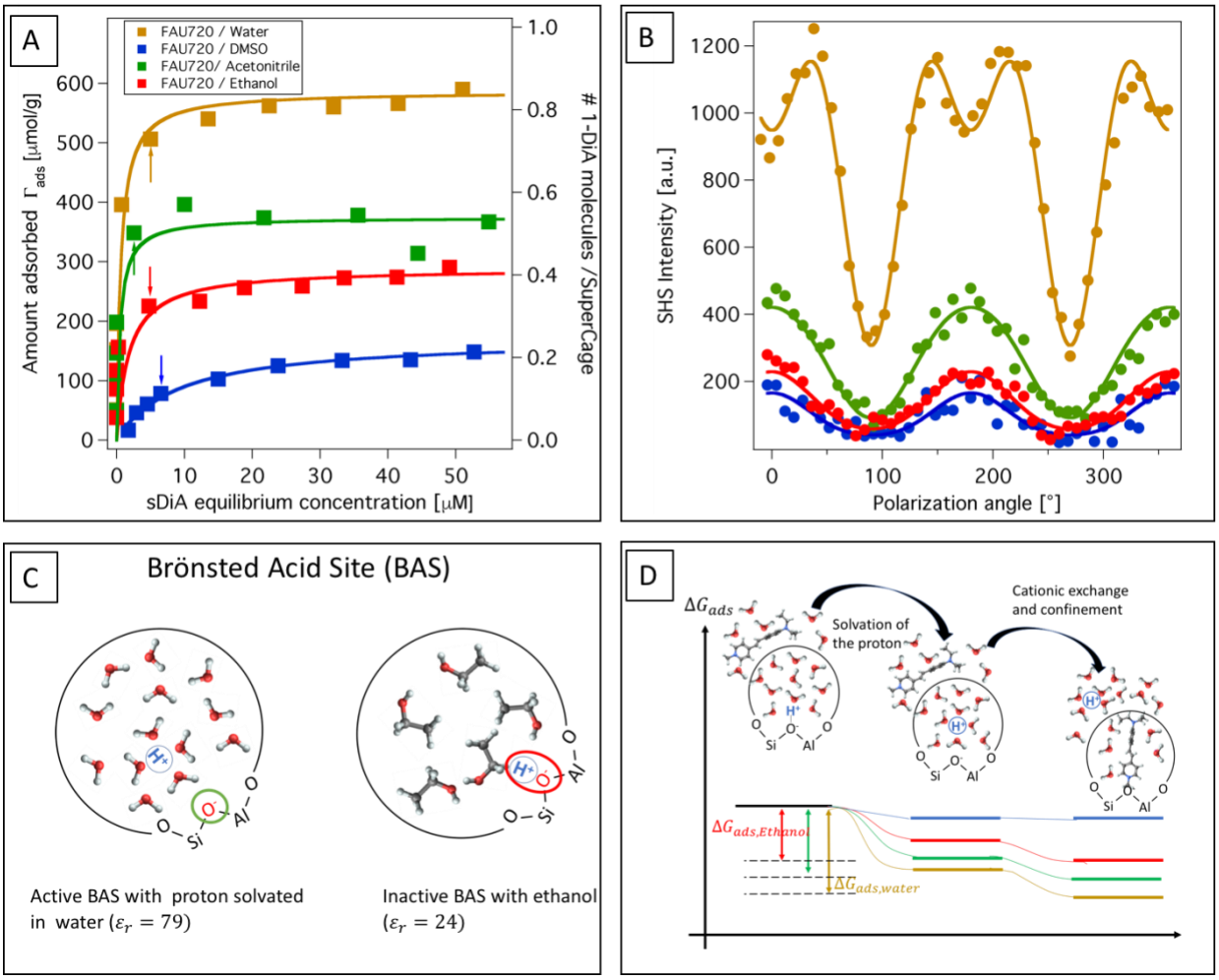

Figure 3. A) Adsorption isotherm for sDiA onto FAU720 with different solvents: water (brown), acetonitrile (green), ethanol (red) and DMSO (blue). B) SHS polarization plot performed at the isotherm shoulder, as indicated with the arrow on graph A. C) Scheme to depict active or inactive Bronsted Acid Site depending on the solvent used. D) Evolution of free enthalpy during the adsorption process.

The impact of the material for the case of ethanol solvent is presented in Figure 4A. The results greatly differ from the water solvent. The adsorption capacity follows monotonically the Si/Al ratio. This shows that the adsorption is limited by the number of active BAS and not by the space available in the framework. Those results confirm that only a small part of the BAS are "active"

with a proton solvated in ethanol. Figures 4B presents the SHS polarization plot for these systems. Those results also confirm that when the material is few filled, no correlation is detected and that I_4 increases with the filling of the material.

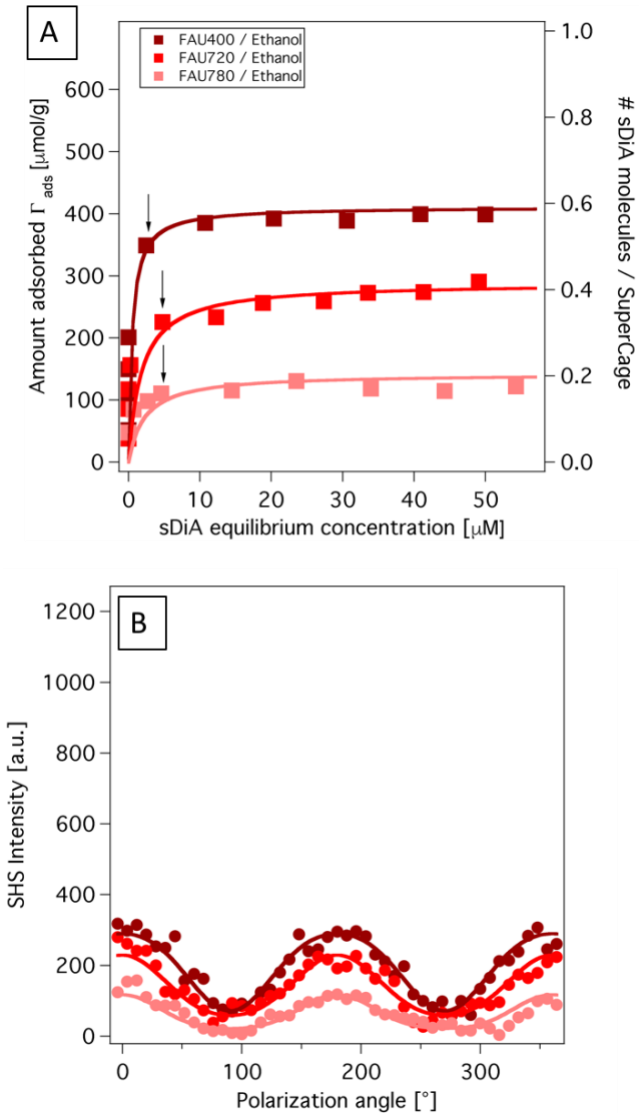

Figure 4. A) Adsorption isotherm for sDiA onto FAU400, FAU720 and FAU780 in ethanol, B) SHS polarization plot performed at the isotherm shoulder, as indicated with the arrow on graph A.

A summary taking into account all the SHS results, is presented in Figure 5. It shows that I_4 quantification draws a distinction between three kind of dye intercalations. For the case of low

adsorption with Γ_{max} lower than 0.4 molecule per SC, the I_4 value is around 0, and thus the system exhibits no correlation between the dye. The molecules don't really interact with the others. For the case with moderate or high filling, i.e. Γ_{max} higher than 0.5 dye per SC, I_4 increase up to -0.25. This evolution shows that long range correlation appears in the system when molecules interact with other located in the immediate surrounding SC. This could induce a percolation phase transition of the intercalated dye and explains the long rang correlation emergence. The last point in Figure 5B represent the case of the FAU400 materials in water. This system exhibits a specific behavior not in line with the other. This is probably explained by the unoccupied sites, which decrease the long range order in the system.

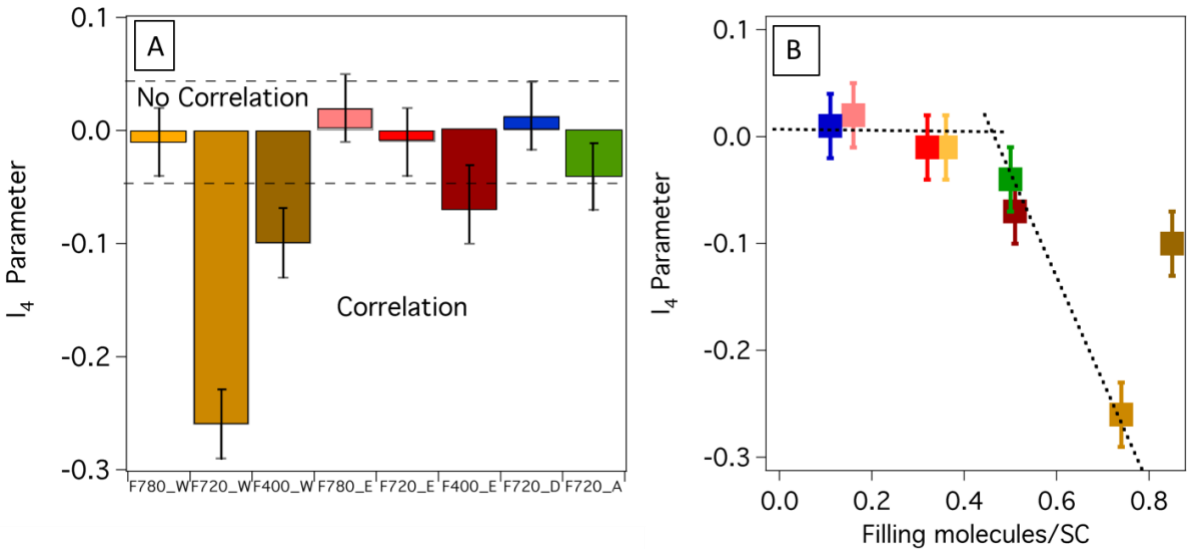

Figure 5. A), I_4 parameters deduced from SHS experiments for sDiA adsorption onto the different Faujasites and various solvent. The acronym in horizontal axis gives the material and solvent (W=Water, E=Ethanol, D=DMSO and A=Acetonitrile). B) I_4 evolution with the loading of the materials. The color code is same as in A) . The dashed lines are guide eyes.

Conclusion

As a conclusion, this work demonstrates that the adsorption process involved in this system is a cation exchange mechanism. The amount adsorbed depends on the number of available exchange sites, with a maximum limit due to the steric hindrance because of the size of the adsorbate. The efficiency of the exchange depends on the ionic properties of the solvent. At high loading, the porous structure of the zeolite leads to long range order and to non-zero values for I_4 parameter. When the number of exchange sites is higher than the maximum achieved loading, unoccupied sites result in a loss of long range order and in a lower value for I_4. The calorimetric measurements also show an increase of the entropic contribution with the unoccupied sites. Finally, this work demonstrates the ability of SHS measurements to probe the organization in buried system. In particular, it opens new perspectives to probe the local order and confinement of molecular inclusion in other class of material, thanks to the SHS measurement of correlations.

ASSOCIATED CONTENT

Supporting Information. Additional information are given about the SHS experimental setup, the 2ω photons reabsorption, the suspension characterization by DLS measurement, and the calculus of the theoretical cationic exchange capacity. The following files are available free of charge.

Funding Sources

Financial support for this work by the ANR project **CAMOMILS (ANR-15-CE21-0002)** is greatly acknowledged.

ACKNOWLEDGMENT

We thank Lotfi Boudjema and Anne Galarneau for regular discussions about the zeolite structure.

ABBREVIATIONS

SHS, Second Harmonic Scattering; BAS, Bronsted Acid site; CEC, Cationic Exchange Capacity, SC, SuperCage.

REFERENCES

1. Li, Y.; Li, L.; Yu, J., Applications of Zeolites in Sustainable Chemistry. *Chem* **2017,** *3* (6), 928-949.
2. Stocker, K.; Ellersdorfer, M.; Lehner, M.; Raith, J. G., Characterization and Utilization of Natural Zeolites in Technical Applications. *BHM Berg- und Hüttenmännische Monatshefte* **2017,** *162* (4), 142-147.
3. Colella, C.; Gennaro, M. d.; Aiello, R., Use of Zeolitic Tuff in the Building Industry. *Reviews in Mineralogy and Geochemistry* **2001,** *45* (1), 551-587.
4. Nakhli, S. A. A.; Delkash, M.; Bakhshayesh, B. E.; Kazemian, H., Application of Zeolites for Sustainable Agriculture: a Review on Water and Nutrient Retention. *Water, Air, & Soil Pollution* **2017,** *228* (12), 464.
5. Misaelides, P., Application of natural zeolites in environmental remediation: A short review. *Microporous and Mesoporous Materials* **2011,** *144* (1), 15-18.
6. Bacakova, L.; Vandrovcova, M.; Kopova, I.; Jirka, I., Applications of zeolites in biotechnology and medicine – a review. *Biomaterials Science* **2018,** *6* (5), 974-989.
7. Shaw, R.; Sharma, R.; Tiwari, S.; Tiwari, S. K., Surface Engineered Zeolite: An Active Interface for Rapid Adsorption and Degradation of Toxic Contaminants in Water. *ACS Applied Materials & Interfaces* **2016,** *8* (19), 12520-12527.
8. Jiang, N.; Shang, R.; Heijman, S. G. J.; Rietveld, L. C., High-silica zeolites for adsorption of organic micro-pollutants in water treatment: A review. *Water Research* **2018,** *144*, 145-161.
9. Samanta, P.; Desai, A. V.; Let, S.; Ghosh, S. K., Advanced Porous Materials for Sensing, Capture and Detoxification of Organic Pollutants toward Water Remediation. *ACS Sustainable Chemistry & Engineering* **2019,** *7* (8), 7456-7478.
10. Wang, S. B.; Peng, Y. L., Natural zeolites as effective adsorbents in water and wastewater treatment. *Chem. Eng. J.* **2010,** *156* (1), 11-24.
11. Wang, S.; Li, H.; Xie, S.; Liu, S.; Xu, L., Physical and chemical regeneration of zeolitic adsorbents for dye removal in wastewater treatment. *Chemosphere* **2006,** *65* (1), 82-87.
12. De Smedt, C.; Ferrer, F.; Leus, K.; Spanoghe, P., Removal of Pesticides from Aqueous Solutions by Adsorption on Zeolites as Solid Adsorbents. *Adsorption Science & Technology* **2015,** *33* (5), 457-485.
13. Martucci, A.; Braschi, I.; Bisio, C.; Sarti, E.; Rodeghero, E.; Bagatin, R.; Pasti, L., Influence of water on the retention of methyl tertiary-butyl ether by high silica ZSM-5 and Y zeolites: a multidisciplinary study on the adsorption from liquid and gas phase. *RSC Adv.* **2015,** *5* (106), 86997-87006.
14. Wang, S. B.; Li, H.; Xu, L. Y., Application of zeolite MCM-22 for basic dye removal from wastewater. *J. Colloid Interface Sci.* **2006,** *295* (1), 71-78.

15. Sarti, E.; Chenet, T.; Stevanin, C.; Costa, V.; Cavazzini, A.; Catani, M.; Martucci, A.; Precisvalle, N.; Beltrami, G.; Pasti, L., High-Silica Zeolites as Sorbent Media for Adsorption and Pre-Concentration of Pharmaceuticals in Aqueous Solutions. *Molecules* **2020,** *25* (15).
16. Noviello, M.; Gattullo, C. E.; Allegretta, I.; Terzano, R.; Gambacorta, G.; Paradiso, V. M., Synthetic zeolite materials from recycled glass and aluminium food packaging as potential oenological adjuvant. *Food Packaging and Shelf Life* **2020,** *26*, 100572.
17. Pagis, C.; Morgado Prates, A. R.; Farrusseng, D.; Bats, N.; Tuel, A., Hollow Zeolite Structures: An Overview of Synthesis Methods. *Chemistry of Materials* **2016,** *28* (15), 5205-5223.
18. Serrano, D. P.; Escola, J. M.; Pizarro, P., Synthesis strategies in the search for hierarchical zeolites. *Chemical Society Reviews* **2013,** *42* (9), 4004-4035.
19. Shamzhy, M.; Opanasenko, M.; Concepción, P.; Martínez, A., New trends in tailoring active sites in zeolite-based catalysts. *Chemical Society Reviews* **2019,** *48* (4), 1095-1149.
20. Grommet, A. B.; Feller, M.; Klajn, R., Chemical reactivity under nanoconfinement. *Nature Nanotechnology* **2020,** *15* (4), 256-271.
21. Dai, J. J.; Zhang, H. B., Recent Advances in Catalytic Confinement Effect within Micro/Meso-Porous Crystalline Materials. *Small* **2021,** *17* (22).
22. Sastre, G.; Corma, A., The confinement effect in zeolites. *Journal of Molecular Catalysis a-Chemical* **2009,** *305* (1-2), 3-7.
23. Varghese, J. J.; Mushrif, S. H., Origins of complex solvent effects on chemical reactivity and computational tools to investigate them: a review. *Reaction Chemistry & Engineering* **2019,** *4* (2), 165-206.
24. Gould, N. S.; Li, S.; Cho, H. J.; Landfield, H.; Caratzoulas, S.; Vlachos, D.; Bai, P.; Xu, B., Understanding solvent effects on adsorption and protonation in porous catalysts. *Nature Communications* **2020,** *11* (1), 1060.
25. Prelot, B.; Lantenois, S.; Charbonnel, M.-C.; Marchandeau, F.; Douillard, J. M.; Zajac, J., What are the main contributions to the total enthalpy of displacement accompanying divalent metal adsorption at the silica-electrolyte interface? *J. Colloid Interface Sci.* **2013,** *396*, 205-209.
26. Bordiga, S.; Lamberti, C.; Bonino, F.; Travert, A.; Thibault-Starzyk, F., Probing zeolites by vibrational spectroscopies. *Chemical Society Reviews* **2015,** *44* (20), 7262-7341.
27. Vimont, A.; Thibault-Starzyk, F.; Daturi, M., Analysing and understanding the active site by IR spectroscopy. *Chemical Society Reviews* **2010,** *39* (12), 4928-4950.
28. Grifoni, E.; Piccini, G.; Lercher, J. A.; Glezakou, V.-A.; Rousseau, R.; Parrinello, M., Confinement effects and acid strength in zeolites. *Nature Communications* **2021,** *12* (1), 2630.
29. Tabacchi, G., Supramolecular Organization in Confined Nanospaces. *ChemPhysChem* **2018,** *19* (11), 1249-1297.
30. Ramamurthy, V., Controlling photochemical reactions via confinement: zeolites. *Journal of Photochemistry and Photobiology C: Photochemistry Reviews* **2000,** *1* (2), 145-166.
31. Van Cleuvenbergen, S.; Smith, Z. J.; Deschaume, O.; Bartic, C.; Wachsmann-Hogiu, S.; Verbiest, T.; van der Veen, M. A., Morphology and structure of ZIF-8 during crystallisation measured by dynamic angle-resolved second harmonic scattering. *Nature communications* **2018,** *9* (1), 3418-3418.
32. Moris, M.; Van Den Eede, M.-P.; Koeckelberghs, G.; Deschaume, O.; Bartic, C.; Van Cleuvenbergen, S.; Clays, K.; Verbiest, T., Harmonic light scattering study reveals structured clusters upon the supramolecular aggregation of regioregular poly(3-alkylthiophene). *Communications Chemistry* **2019,** *2* (1), 130.

33. Duboisset, J.; Brevet, P.-F., Salt-induced Long-to-Short Range Orientational Transition in Water. *Physical Review Letters* **2018,** *120* (26), 263001.
34. Gassin, P.-M.; Prelot, B.; Grégoire, B.; Martin-Gassin, G., Second-Harmonic Scattering in Layered Double Hydroxide Colloids: A Microscopic View of Adsorption and Intercalation. *Langmuir* **2018,** *34* (40), 12206-12213.
35. Gassin, P.-M.; Prelot, B.; Gregoire, B.; Martin-Gassin, G., Second-Harmonic Scattering Can Probe Hydration and Specific Ion Effects in Clay Particles. *The Journal of Physical Chemistry C* **2020,** *124* (7), 4109-4113.
36. Pardon, A.; Bonhomme, O.; Gaillard, C.; Brevet, P.-F.; Benichou, E., Nonlinear optical signature of nanostructural transition in ionic liquids. *Journal of Molecular Liquids* **2021,** *322*, 114976.
37. Chen, Y.; Okur, H. I.; Gomopoulos, N.; Macias-Romero, C.; Cremer, P. S.; Petersen, P. B.; Tocci, G.; Wilkins, D. M.; Liang, C.; Ceriotti, M.; Roke, S., Electrolytes induce long-range orientational order and free energy changes in the H-bond network of bulk water. *Science Advances* **2016,** *2* (4), e1501891.
38. Tocci, G.; Liang, C.; Wilkins, D. M.; Roke, S.; Ceriotti, M., Second-Harmonic Scattering as a Probe of Structural Correlations in Liquids. *The Journal of Physical Chemistry Letters* **2016,** *7* (21), 4311-4316.
39. Kim, H. S.; Lee, S. M.; Ha, K.; Jung, C.; Lee, Y.-J.; Chun, Y. S.; Kim, D.; Rhee, B. K.; Yoon, K. B., Aligned Inclusion of Hemicyanine Dyes into Silica Zeolite Films for Second Harmonic Generation. *Journal of the American Chemical Society* **2004,** *126* (2), 673-682.
40. van der Veen, M. A.; Sels, B. F.; De Vos, D. E.; Verbiest, T., Localization of p-nitroaniline chains inside zeolite ZSM-5 with second-harmonic generation microscopy. *J Am Chem Soc* **2010,** *132* (19), 6630-1.
41. Boudjema, L.; Aarrass, H.; Assaf, M.; Morille, M.; Martin-Gassin, G.; Gassin, P.-M., PySHS: Python Open Source Software for Second Harmonic Scattering. *Journal of Chemical Information and Modeling* **2020,** *60* (12), 5912-5917.
42. Duboisset, J.; Rondepierre, F.; Brevet, P.-F., Long-Range Orientational Organization of Dipolar and Steric Liquids. *The Journal of Physical Chemistry Letters* **2020,** *11* (22), 9869-9875.
43. Zajac, J., Calorimetry at the Solid–Liquid Interface. In *Calorimetry and Thermal Methods in Catalysis*, Auroux, A. E., Ed. Springer Series in Materials Science: 2013; pp 197-270.
44. Gassin, P.-M.; Bellini, S.; Zajac, J.; Martin-Gassin, G., Adsorbed Dyes onto Nanoparticles: Large Wavelength Dependence in Second Harmonic Scattering. *The Journal of Physical Chemistry C* **2017,** *121* (27), 14566-14571.
45. Houbrechts, S.; Clays, K.; Persoons, A.; Pikramenou, Z.; Lehn, J.-M., Hyper-Rayleigh scattering investigation of nitrobenzyl pyridine model compounds for optical modulation of the hyperpolarisability. *Chemical Physics Letters* **1996,** *258* (3), 485-489.
46. Kondo, J. N.; Nishitani, R.; Yoda, E.; Yokoi, T.; Tatsumi, T.; Domen, K., A comparative IR characterization of acidic sites on HY zeolite by pyridine and CO probes with silica–alumina and γ-alumina references. *Physical Chemistry Chemical Physics* **2010,** *12* (37), 11576-11586.
47. Liu, Y., Is the Free Energy Change of Adsorption Correctly Calculated? *Journal of Chemical & Engineering Data* **2009,** *54* (7), 1981-1985.

TOC